

To Cite: Aydın, M. & Yakut, O. (2023). Implementation of Sliding Surface Moving Anfis Based Sliding Mode Control to Rotary Inverted Pendulum. *Journal of the Institute of Science and Technology*, 13(1), 1165-1175.

Implementation of Sliding Surface Moving Anfis Based Sliding Mode Control to Rotary Inverted Pendulum

Muhammet AYDIN^{1*}, Oğuz YAKUT²

Highlights:

- It includes the anfis-based moving sliding mode control of the rotational inverted pendulum system.
- The unstable upper balance point of the rotational inverted pendulum system and the control of the rotating arm are realized.
- Combining control structures, a control structure that has not been tried before was applied

ABSTRACT:

This study covers the control of the pendulum angle by taking into account the dynamic equations and motor dynamics of the rotary inverted pendulum system, with the help of state variables in the Matlab program, by using the sliding mode control method with sliding surface moving and the adaptive neural fuzzy inference system together. The sliding mode control method with a changing sliding surface is a part of the control structure. The slope of the sliding surface was calculated using the adaptive neural fuzzy inference technique. The optimum values of the coefficients in the adaptive neural-fuzzy inference system structure have been calculated by genetic algorithm. The finding of the coefficients, the sum of the squares of the errors chosen as the objective function. The input of the adaptive neural fuzzy inference system structure consists of the error of the pendulum and the derivative of the error of the pendulum. The gradient of the sliding surface of the sliding mode control structure is the output of the adaptive neural fuzzy inference system structure. According to the findings, the pendulum angle achieved the appropriate reference value after 1.5 seconds, with an error of around zero. It obtained that the engine torque value reaches up to 50 Nm. From here, it is seen that the motor torque values used in practical applications and the motor torque values as a result of this study overlap.

Keywords:

- Rotary inverted pendulum
- Sliding mode control
- Anfis
- Moving sliding surface

¹ Muhammet AYDIN ([Orcid ID: 0000-0003-2746-9477](https://orcid.org/0000-0003-2746-9477)), Fırat University, Faculty of Engineering, Department of Mechatronics Engineering, Elazığ, Türkiye

² Oğuz YAKUT ([Orcid ID: 0000-0002-0986-1435](https://orcid.org/0000-0002-0986-1435)), Fırat Üniversitesi, Faculty of Engineering, Department of Mechatronics Engineering, Elazığ, Türkiye

Corresponding Author: Muhammet AYDIN, e-mail: muhammeta@firat.edu.tr

INTRODUCTION

In control applications, the control of the inverted pendulum system is undoubtedly momentous because the inverted pendulum system forms the basis of most systems. For this reason, inverted pendulum systems are one of the most suitable systems being controlled. Different structures created to date contain inverted pendulum systems. Some of them are the single and double-rotating inverted pendulum systems (Awtar et al., 2002; Krishen and Becerra, 2006), the single inverted pendulum on a cart (Bugeja, 2003), and the double inverted pendulum on a cart (Zhong and Röck, 2001).

One of the most widely used pendulum systems due to its cheap and manufacturing easily is the rotary inverted pendulum system. The Great setting for studying the control of non-linear and indirectly driven unstable systems is Rotary Inverted Pendulum System. The fact that it is easier to manufacture and more economical than the trolley-type inverted pendulum has made it highly preferred recently. The rotary inverted pendulum system consists of two stiff moving parts. The horizontal cylindrical arm is the first limb. The rotating driving element attached to the horizontal cylindrical arm allows for the arm's motion. The other, which is the vertically moving shaft, is the pendulum. The pendulum's swinging is provided by the movement backward and forward of the horizontal cylindrical arm in this system; the pendulum is stabilized at the upper unstable balance point (Yan, 2003; Kuo et al., 2009).

In the studies presented so far in the literature for the angle control of the rotating inverted pendulum system seen in Figure 1, classical control methods such as PID (Kuo et al., 2009), PI, PD (Altinoz et al., 2010), adaptive control methods with sliding mode control (Bogdanov, 2004; Wang, 2009; Aydin et al., 2019), fuzzy control (Krishen and Becerra, 2006), sliding mode control (Khanesar et al., 2007), particle swarm optimization based PID control (Sugie and Fujimoto 1998; Bogdanov, 2004; Hassanzadeh and Mobayen, 2008; Sukontanakarn and Parnichkun 2009) and there are control studies sliding mode control methods via the artificial neural network (Aydin et al., 2019).

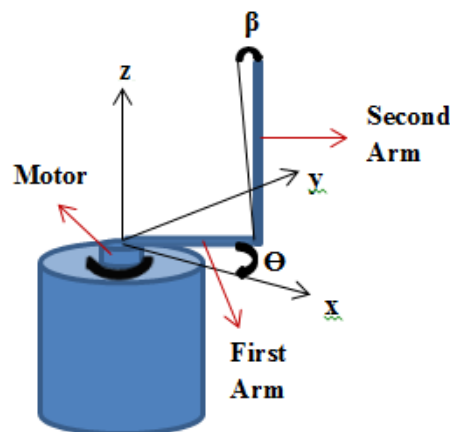


Figure 1. The rotary inverted pendulum system

Especially in recent years, development of a Neuro-Fuzzy Friction Estimation Model used to estimate the joint friction coefficients of a Triple Link Rotary Inverted Pendulum system (Hazem et al., 2020), controlled of a rotary inverted pendulum by adaptive techniques (Nath and Dewan, 2017), performing stability control of double link rotary inverted pendulum with Fuzzy-LQR and Fuzzy-LQG methods (Hazem et al., 2020), developing of a fuzzy logic controller for rotary inverted pendulum (Le et al., 2018), controlling the rotary inverted pendulum with incremental sliding mode control (Hong et al., 2019), a comparative analysis of the linear quadratic regulator and sliding mode control results for the rotating inverted pendulum (Nath and Dewan, 2018), performing of model-free sliding mode

stabilizing control of the actual rotary inverted pendulum (Yiğit, 2017), developing of numerical design method by using non linear sliding mode control method for Rotary inverted pendulum (Cui, 2019), comparing the PID and sliding mode control results of the rotating inverted pendulum system using PLC (Howimanporn et al., 2020), pole placement controller applied to rotary inverted pendulum system (Muñoz-Poblete, 2018), performing of a rotary inverted pendulum real-time stability control using an LQR-based sliding mode controller (Chawla and Singla, 2021), performing of an adaptive neural network-based control of the rotary inverted pendulum with oscillation compensation (Zabihifar et al., 2020) studies have come to the fore.

In this study, using the non-linear model of the rotary inverted pendulum system, the pendulum angle is controlled by the sliding mode control method by the changing sliding surface taking advantage of the adaptive neural fuzzy inference system (anfis). The slope of the sliding surface was obtained using an anfis structure. The optimum values of the coefficients in the anfis are calculated via the genetic algorithm.

MATERIALS AND METHODS

Conversion of Rotary Inverted Pendulum System to State Variables

In previous studies, the equations of motion of the rotary inverted pendulum system were obtained. The equations of motion gave in Equations 1 and 2 in this study.

The equation of motion for θ :

$$(m_1L_1^2 + I_1 + m_2L_1 + m_2L_2^2 \sin^2\beta)\ddot{\theta} + m_2L_1L_2 \cos\beta\ddot{\beta} - m_2L_1L_2 \sin\beta\dot{\beta}^2 + 2m_2L_2^2 \sin\beta \cos\beta \dot{\beta}\dot{\theta} = \tau - b_1\dot{\theta} \tag{1}$$

The equation of motion for β :

$$m_2L_1L_2 \cos\beta\ddot{\theta} + (m_2L_2^2 + I_2)\ddot{\beta} - m_2L_2^2 \sin\beta \cos\beta \dot{\theta}^2 - m_2gL_2 \sin\beta = -b_2\dot{\beta} \tag{2}$$

The following equations are generated if the expressions $\ddot{\theta}$ and $\ddot{\beta}$ taken away from the equations of motion.

$$\ddot{\theta} = \frac{(m_2L_2^2 + I_2)(b_1\dot{\theta} - \tau - m_2L_1L_2 \sin\beta\dot{\beta}^2 + 2m_2L_2^2 \sin\beta \cos\beta \dot{\beta}\dot{\theta})}{(m_2L_1L_2 \cos\beta)^2 - (m_2L_2^2 + I_2)(m_1L_1^2 + I_1 + m_2L_1 + m_2L_2^2 \sin^2\beta)} - \frac{m_2L_1L_2 \cos\beta(b_2\dot{\beta} - m_2L_2^2 \sin\beta \cos\beta \dot{\theta}^2 - m_2gL_2 \sin\beta)}{(m_2L_1L_2 \cos\beta)^2 - (m_2L_2^2 + I_2)(m_1L_1^2 + I_1 + m_2L_1 + m_2L_2^2 \sin^2\beta)} \tag{3}$$

$$\ddot{\beta} = \frac{(m_1L_1^2 + I_1 + m_2L_1 + m_2L_2^2 \sin^2\beta)(b_2\dot{\beta} - m_2L_2^2 \sin\beta \cos\beta \dot{\theta}^2 - m_2gL_2 \sin\beta)}{(m_2L_1L_2 \cos\beta)^2 - (m_2L_2^2 + I_2)(m_1L_1^2 + I_1 + m_2L_1 + m_2L_2^2 \sin^2\beta)} - \frac{m_2L_1L_2 \cos\beta(b_1\dot{\theta} - \tau - m_2L_1L_2 \sin\beta\dot{\beta}^2 + 2m_2L_2^2 \sin\beta \cos\beta \dot{\beta}\dot{\theta})}{(m_2L_1L_2 \cos\beta)^2 - (m_2L_2^2 + I_2)(m_1L_1^2 + I_1 + m_2L_1 + m_2L_2^2 \sin^2\beta)} \tag{4}$$

The equation of motion of the first arm motor can write as follows. Here, V_a is the motor supply voltage and the control signal, K_b is the back electromotive voltage coefficient, N is the gear ratio, R is the motor winding ohmic resistance, L is the motor inductance coefficient, and i is the electrical current flowing through the motor windings.

$$\frac{di}{dt} = \frac{V_a - Ri}{L} - \frac{K_b\dot{\theta}}{LN} \tag{5}$$

If the expressions in the equations are converted to state variables;

$$\theta = x(1) \tag{6}$$

$$\dot{\theta} = x(2) \quad (7)$$

$$\beta = x(3) \quad (8)$$

$$\dot{\beta} = x(4) \quad (9)$$

$$\frac{di}{dt} = x(5) \quad (10)$$

is obtained as. If the motor control torque is;

$$\tau = \frac{K_t i}{N} \quad (11)$$

It is calculated in the form. Where K_t is the motor torque coefficient.

The Anfis-based moving sliding mode control approach implemented to the rotary inverted pendulum system employs these state variables with the Matlab program. It will make sure that the pendulum angle reaches the specified zero reference point with the control mechanism.

System parameters:

Table 1. System parameters and their values

Parameter	Value
m_1	0.15 kg
m_2	0.1 kg
L_1	0.4 m
L_2	0.4 m
b_1	0.01 N s m ⁻¹
b_2	0.01 N s m ⁻¹
I_1	0.0248 kg m ⁴
I_2	0.00386 kg m ⁴
L	0.1 henry
R	1.4 Ohm
K_t	0.25
K_b	0.05
N	1/20

Sliding Surface Moving Anfis-Based Design of Sliding Mode Control

A non-linear and reliable control strategy is sliding mode control. Compared to other control methods, it is a method that is not affected by external disturbances. Thanks to the oscillations on the sliding surface to reach the desired reference, the result reaches quickly with high accuracy (Young et al., 1999). Because the system parameters are unknown or constantly changing and external disturbances are affecting the system, long-term controllability is possible with the sliding mode control as long as the system's limit values are understood.

While performing the sliding mode control, the sliding surface must first determine, and a control rule must create to reach the determining sliding surface. The reaching time is the amount of time required to reach the sliding surface. The reaching mode is the area of the phase trajectory in this layer. The system is vulnerable to parameter uncertainty and outside noise when in the reaching mode (Edwards and Spurgeon, 1998). When the sliding surface is reached, the slip mode begins, in which the system's course is unaffected by ambiguous parameters and outside influences. The oscillations around the equilibrium point that the system wishes to reach in sliding mode control applications lead to chattering, which shows the unmodeled high-frequency dynamics of the system.

A sliding mode control expression with a sign function can write as in Equation 12. Here S is the sliding surface function, e is the error of the system response, and de is the error variation to the time expressed in Equation 13.

$$U = -k \operatorname{sign}(S) \tag{12}$$

$$S = C e + de \tag{13}$$

Figure 2 illustrates the slope of the sliding surface. The coefficient C in the equation represents this slope (23).

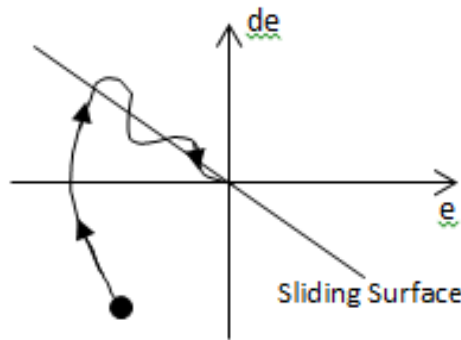


Figure 2. Sliding surface

The most suitable value of this stated slope must choose to increase the controller's success. The coefficients of the sliding surface slope are regarded as moving for this investigation. The slope coefficient C included using the Anfis structure. The Anfis structure introduces using the error of the pendulum angle and the derivative of the pendulum error. The output value of the sliding mode control is equal to the slope coefficient of the sliding surface. The Genetic algorithm is used to determine the parameters' optimum numbers in the Anfis. The optimum values of the base coefficients of the membership functions in the fuzzy logic structure calculate using a genetic algorithm in Matlab. The parameters preferred as FitnessLimit 1e-10, Generations 50, and PopulationSize 15 in the genetic algorithm structure. Figure 3 shows the block diagram, where the controller coefficients are optimized by the genetic algorithm technique.

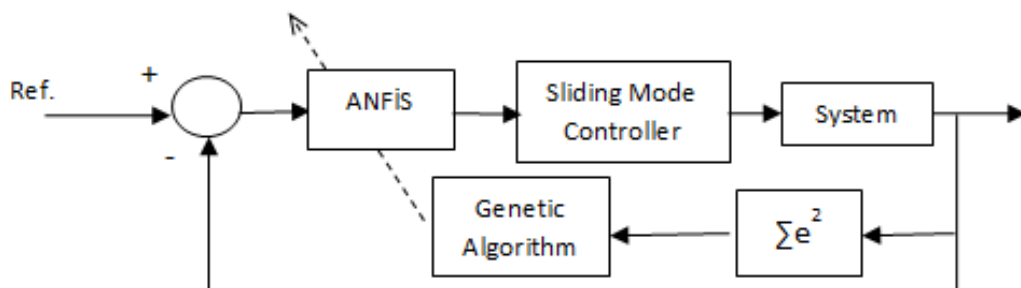


Figure 3. Controller block

The "Sugeno" type is a frequently used fuzzy controller in the Anfis structure discussed in this study. The big difference that distinguishes the Sugeno-type structure and the Mamdani-type structure is that the outputs shown in the rules are expressed as functions of the input variables, not as fuzzy sets.

The addition of fuzzy logic principles to artificial neural networks provides the creation of a system that can handle uncertainties and also generalize like artificial neural networks.

The Anfis structure consists of the blurring layer, the two hidden layers, the function layer, and the clarification layer as seen in Figure 4. In the blurring layer, the input variables transform into fuzzy sets. Each processing unit in this layer corresponds to a fuzzy set, and the processing unit output is a membership function. In the blurring layer, the position error e of the pendulum and the derivative of the error for the time used as inputs to define the fuzzy working region, and three membership functions selected for inputs.

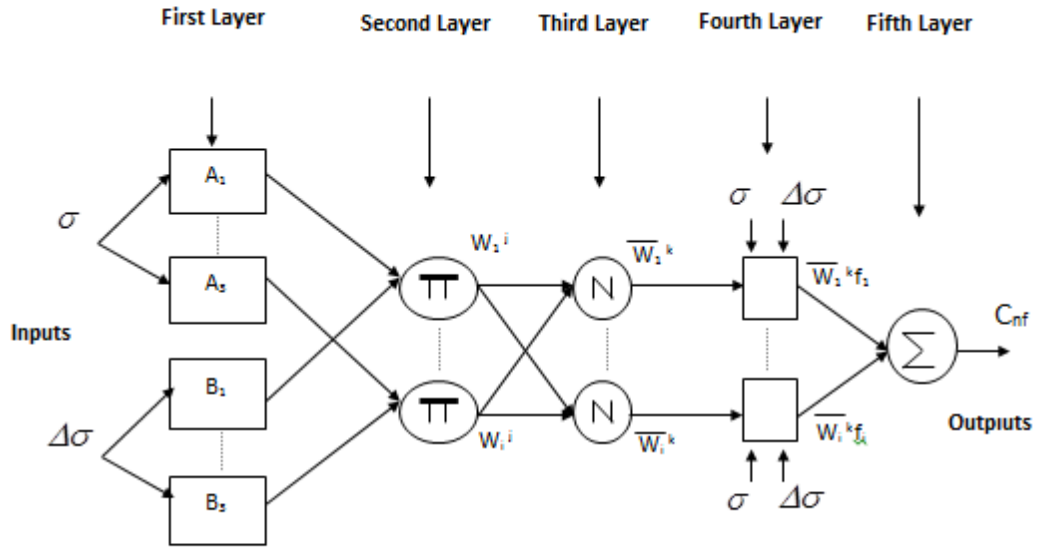


Figure 4. The network-based fuzzy logic structure

The Gause membership function is preferred for this. Accordingly, these membership functions are as given in equations 14 and 15.

$$\mu_{A_i}(\sigma) = e^{-\left(\frac{\sigma - c_i}{a_i}\right)^2} \text{ for } i=1,2,3, \tag{14}$$

$$\mu_{B_i}(\Delta\sigma) = e^{-\left(\frac{\Delta\sigma - c_i}{a_i}\right)^2} \text{ for } i=1,2,3, \tag{15}$$

The algebraic product with the following equation can use to determine the precision levels of the rules in the second layer.

$$w_i^j = \mu_{A_i}(\sigma)\mu_{B_{Ai}}(\Delta\sigma) \tag{16}$$

The ratio of one rule's precision to another can view as the normalizing process. It reveals how the rule affects the output term of all the rules. The following processes perform in the third layer of the network.

$$\bar{w}_i^k = \frac{w_i^j}{w_1^j + w_2^j + w_3^j + \dots} \text{ for } i=1,2,3, \tag{17}$$

Each normalized rule is multiplied by its output function at layer 4 using the following expression.

$$\bar{w}_i^k f_i = w_i^k (p_i \sigma^T + q_i \Delta\sigma^T) \tag{18}$$

Where p and q coefficients are linear parameters of the functions used in the function layer.

The clarification layer is the fifth layer, where the clarification process is carried out by the center of gravity method, and the output is formed as follows.

$$\text{Output}_{5,i} = \sum_i \bar{w}_i^k f_i = \frac{\sum_i w_i^k f_i}{\sum_i w_i^k} \quad (19)$$

This digital output produced by the Anfis structure is the slip surface slope value of the sliding mode controller.

In the input layer of the created Anfis, it was deemed appropriate to choose three membership functions, equal numbers for each input. The optimum values of all 45 parameters of the designed controller were found using the genetic algorithm technique. The mean square of errors is defined as the performance index of the system preferred for the fitness function being used in determining the optimum values of the controller parameters.

$$E(k) = \frac{1}{2} e^2(k) \quad (20)$$

The sign function in the sliding mode control expression causes the control signal to chatter. Various function types are used instead of this sign function to solve this problem. The widely used saturation function was chosen to replace the sign function in this study. As a result, equation 21's equation for the sliding mode control expression with saturation function was obtained. The epsilon value in the equation was found to be 39.87 by the genetic algorithm.

$$U = -k \cdot \text{sat}\left(\frac{s}{\text{epsilon}}\right) \quad (21)$$

RESULTS AND DISCUSSION

Figure 5 illustrates how the first arm attached to the motor's angular location varies over time. It shifted direction within the first few seconds after beginning at zero. Swinging the pendulum higher is the expected thing.

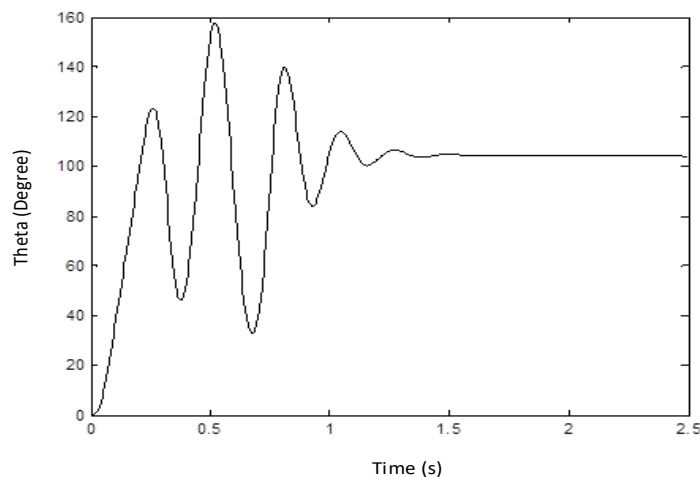


Figure 5. Variation of theta angle with the time

The first arm's angular velocity showed in the graph in Figure 6. It can observe that the angular velocity value oscillates and reaches a maximum of 23 rad/s before stabilizing at 0 rad/s. A graph depicting the change in pendulum angle over time showed in Figure 7. The unstable upper balance point is where the pendulum must come to a stop. As a result, the desired zero reference point must reach by the pendulum angle.

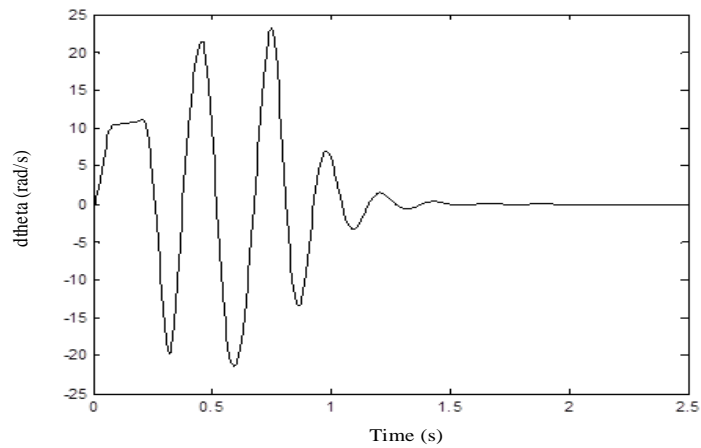


Figure 6. Angular velocity change of the first arm to time

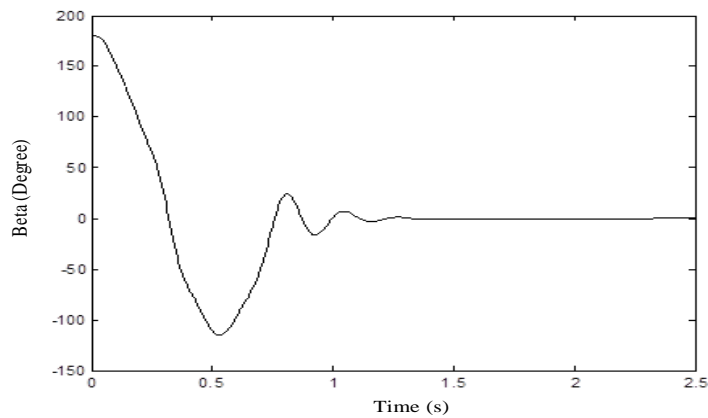


Figure 7. Variation of beta angle (pendulum angle) with the time

The pendulum takes around 1.5 seconds to reference value, as shown in the image. Figure 8 depicts the pendulum's angular velocity as it changes over time. The graph shows that the pendulum's angular speed reaches zero after 1.5 seconds.

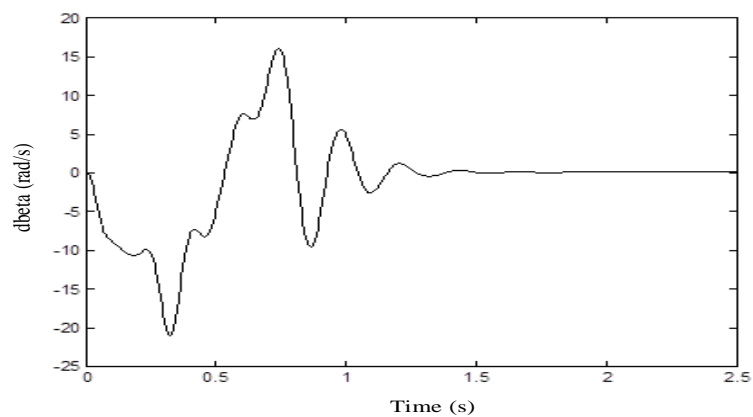


Figure 8. Angular velocity change of the pendulum to the time

In Figures 9 and 10, the torque value required applied to the first arm and the slope value of the sliding surface gave, respectively. When the DC motor torque graph in When Figure 9 is looked at, it is evident that a motor torque of about 50 Nm will be enough to raise the pendulum to the necessary reference point. This torque value is suitable for actual applications, it might assert. After about 1.5 seconds, the engine torque reaches zero.

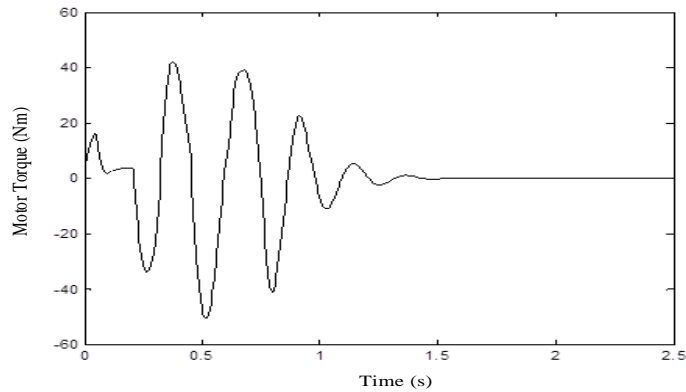


Figure 9. Variation of DC motor's torque with the time

When the sliding surface slope graph in Figure 10 is examined, it has seen that it takes values between 0-130. Figure 11 shows the time change of the supply voltage applied to the DC motor as a control signal. It can also see from the graph that the DC motor supply voltage source is limited to 12 volts.

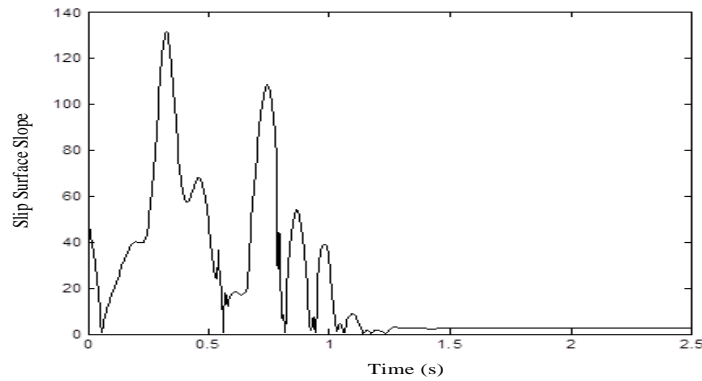


Figure 10. Slip surface slope graph

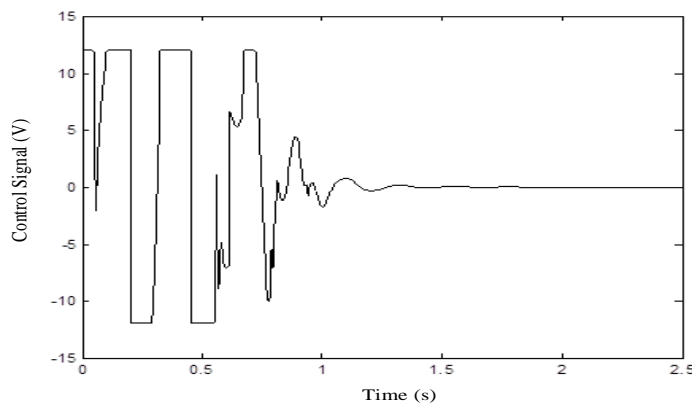


Figure 11. Graph of DC motor control signal with the time

The variation of the current passing through the DC motor windings with the time is shown in Figure 12. It saw that the current drawn by the motor reached zero after about 1.5 seconds. It has seen from the graph that the maximum current drawn by the engine is 10 Amperes. Table 2 compares the result of the study presented in this research paper with those of two previous works (Aydin et al., 2019; Aydin and Yakut, 2022). As noted in the table, the pendulum angle of the system in the current study with 1.35 s settling time produced a better settling time from network-based MSMC. The fuzzy-

based MSMC has the fastest settling time of the three algorithms at 0.9 seconds. The current study had moderate success.

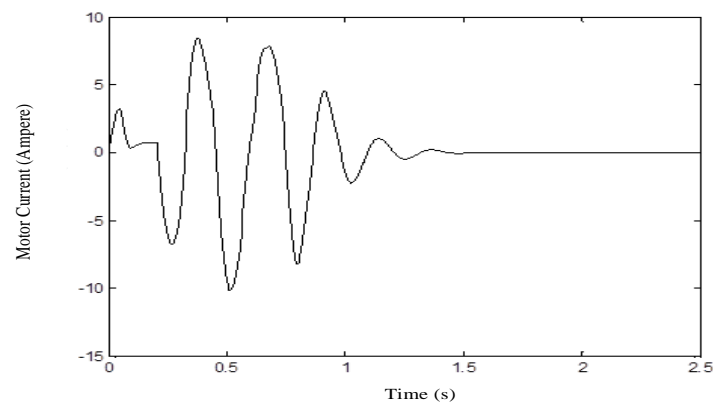


Figure 12. Graph of DC motor current with the time

Table 2. Comparison of between works in the literature and the present study

	Method	Settling time (s)
Pendulum angle settling-time values	Network-based MSMC	3.0
	Fuzzy-based MSMC	0.90
	Anfis-based MSMC (Present study)	1.35

CONCLUSION

This study is related to the single degree of freedom rotary inverted pendulum system's non-linear dynamic model. The Matlab program was performed to control the pendulum angle using state variables over motor dynamics and dynamic equations. The system is subject to the moving sliding mode control technique to control it. The Anfis provides the changing of the sliding surface's slope using the moving sliding mode control method. A genetic algorithm is used to determine the coefficients of the Anfis structure. After the investigation, it notes that the control signal has reached zero, the error is zero, and the pendulum has achieved the appropriate reference value in roughly 1.5 seconds. The motor torque value reaches a maximum of 50 Nm, and the motor current value to 10 Amperes. The results showed that if these values think while selecting the motor in real applications, the rotary inverted pendulum system will operate smoothly with its Anfis structure and moving sliding mode control. In future works, the controller structure preferred here can apply to the double-rod and triple-rod rotary inverted pendulum system.

Conflict of Interest

The article authors declare that there is no conflict of interest between them.

Author's Contributions

The authors declare that they have contributed equally to the article.

REFERENCES

- Altinoz, OT, Yilmaz, AE, Weber, GW, 2010. Chaos Particle Swarm Optimized Pid Controller for the Inverted Pendulum System. Second International Conference on Engineering Optimization, 6-9 September 2010, Lisbon, Portugal.
- Awtar, S, King, N, Allen, T, Bang, I, Hagan, M, Skidmore, D, Craig, K, 2002. Inverted Pendulum Systems: Rotary and Arm-Driven-a Mechatronic System Design Case Study. *Mechatronics*, 12 (2): 357-370.
- Aydin, M, Yakut, O, Tutumlu, H, 2019. Implementation of the Network-Based Moving Sliding Mode Control Algorithm to the Rotary Inverted Pendulum System. *Journal of Engineering and Technology*, 3 (1): 32-41.
- Aydin, M, Yakut, O, 2022. Application of Fuzzy Sliding Mode Control with Moving Sliding Surface to Rotary Inverted Pendulum. *Journal of Advanced Research in Natural and Applied Sciences*, 8 (3).

- Bogdanov, A, 2004. Optimal Control of a Double Inverted Pendulum on a Cart. Health and Science University Technical Report. CSE-04-006, Oregon Graduate Institute School of Science and Engineering, Oregon, United States of America.
- Bugeja, M, 2003. Non-linear Swing-up and Stabilizing Control of an Inverted Pendulum System. *Computer as a Tool*, 2: 437-441.
- Chawla, I, Singla, A, 2021. Real-time Stabilization Control of a Rotary Inverted Pendulum Using Lqr-based Sliding Mode Controller. *Arabian Journal for Science and Engineering*, 46 (3): 2589-2596.
- Cui, J, 2019. Numerical Design Method for Nonlinear Sliding Mode Control of Inverted Pendulum. 38th Chinese Control Conference, 27-29 July 2019, Guangzhou, China.
- Edwards, C, Spurgeon, S, 1998. *Sliding Mode Control: Theory and Applications*. Chemical Rubber Company Press.
- Hassanzadeh, I, Mobayen, S, 2008. Pso-based Controller Design for Rotary Inverted Pendulum System. *Journal of Applied Sciences*, 8 (16): 2907-2912.
- Hazem, ZB, Fotuhi, MJ, Bingül, Z, 2020. A Comparative Study of the Joint Neuro-Fuzzy Friction Models for a Triple Link Rotary Inverted Pendulum. *Institute of Electrical and Electronics Engineers Access*, 8: 49066-49078.
- Hazem, ZB, Fotuhi, MJ, Bingül, Z, 2020. Development of a Fuzzy-lqr and Fuzzy-lqg Stability Control for a Double Link Rotary Inverted Pendulum. *Journal of the Franklin Institute*, 357 (15): 10529-10556.
- Hong, GB, Nguyen, HT, Nguyen, MT, Hoang Le, TT, Hai Nguyen, VD, 2019. Trajectory Tracking for Futura Pendulum by Incremental Sliding Mode Control. *Robotica and Management*, 24 (1).
- Howimanporn, S, Chookaew, S, Silawatchananai, C, 2020. Comparison between Pid and Sliding Mode Controllers for Rotary Inverted Pendulum Using Plc. Fourth International Conference on Automation, Control, and Robots, 11-13 October 2020, Roma, Italy.
- Khanesar, MA, Teshnehlab, M, Shoorehdeli, MA, 2007. Sliding Mode Control of Rotary Inverted Pendulum. 2007 Mediterranean Conference on Control and Automation, 27-29 June 2007, Athens, Greece.
- Krishen, J, Becerra, VM, 2006. Efficient Fuzzy Control of a Rotary Inverted Pendulum Based on Lqr Mapping. 2006 Institute of Electrical and Electronics Engineers Conference on Computer Aided Control System Design, 2006 Institute of Electrical and Electronics Engineers International Symposium on Intelligent Control, 4-6 October 2006, Munich, Germany.
- Kuo, TC, Huang, YJ, Hong, BW, 2009. Adaptive Pid with Sliding Mode Control for the Rotary Inverted Pendulum System. 2009 Institute of Electrical and Electronics Engineers / American Society of Mechanical Engineers International Conference on Advanced Intelligent Mechatronics, 14-17 July 2009, Singapore.
- Le, TTH, Vo, AK, Van Nguyen, T, Vu, DH, Tran, MS, 2018. Fuzzy Controller for Rotary Inverted Pendulum. *Robotica and Management*, 23 (2).
- Muñoz-Poblete, C, 2018. Pole Placement Controller Applied to a Rotary Inverted Pendulum System. A didactic view. 2018 Institute of Electrical and Electronics Engineers International Conference on Automation/XXIII Congress of the Chilean Association of Automatic Control 17-19 October 2018, Chile.
- Nath, K, Dewan, L, 2017. Control of a Rotary Inverted Pendulum via Adaptive Techniques. 2017 International Conference on Emerging Trends in Computing and Communication Technologies, 17-19 November 2017, Dehradun, India.
- Nath, K, Dewan, L, 2018. A Comparative Analysis of Linear Quadratic Regulator and Sliding Mode Control for a Rotary Inverted Pendulum. 2018 International Conference on Recent Trends in Electrical, Control, and Communication, 20-22 March 2018, Malaysia.
- Stimac, AK, 1999. Standup and Stabilization of the Inverted Pendulum, Massachusetts Institute of Technology, Department of Mechanical Engineering, Doctor of Philosophy Thesis (Printed).
- Sugie, T, Fujimoto, K, 1998. Controller Design for an Inverted Pendulum Based on Approximate Linearization. *International Journal of Robust and Nonlinear Control: International Federation of Automatic Control-Affiliated Journal*, 8 (7): 585-597.
- Sukontanakarn, V, Parnichkun, M, 2009. Real-time Optimal Control for Rotary Inverted Pendulum. *American Journal of Applied Sciences*, 6 (6): 1106.
- Wang, W, 2009. Adaptive Fuzzy Sliding Mode Control for Inverted Pendulum. 2009 International Symposium on Computer Science and Computational Technology, 29-31 August 2009, Vancouver, Canada.
- Yan, Q, 2003. Output Tracking of Underactuated Rotary Inverted Pendulum by Nonlinear Controller. 42nd Institute of Electrical and Electronics Engineers International Conference on Decision and Control, 9-12 December 2003, Maui, United States of America.
- Yiğit, İ, 2017. Model Free Sliding Mode Stabilizing Control of a Real Rotary Inverted Pendulum. *Journal of Vibration and Control*, 23 (10): 1645-1662.
- Young, KD, Utkin, VI, Ozguner, U, 1999. A Control Engineer's Guide to Sliding Mode Control. *Institute of Electrical and Electronics Engineers Transactions on Control Systems Technology*, 7 (3): 328-342.
- Zhong, W, Rock, H, 2001. Energy and Passivity Based Control of the Double Inverted Pendulum on a Cart. 2001 Institute of Electrical and Electronics Engineers International Conference on Control Applications, 5-7 September 2001, Mexico City, Mexico.
- Zabihifar, SH, Yushchenko, AS, Navvabi, H, 2020. Robust Control Based on Adaptive Neural Network for Rotary Inverted Pendulum with Oscillation Compensation. *Neural Computing and Applications*, 32 (18): 14667-14679.